

Evaluating Vegetation Modeling in Earth System Models with Machine Learning Approaches

Ranjini Swaminathan^{1,2}, Tristan Quaife^{1,2} and Richard Allan^{1,2}

¹University of Reading

²National Centre for Earth Observation

Key Points:

- A Machine Learning framework to advance our understanding of the terrestrial carbon cycle in Earth System Models or ESMs is proposed
- Differences in the relative importance of atmospheric drivers of gross primary productivity highlights differences across models
- A method to attribute differences in productivity estimates from ESMs due to process representation versus atmospheric forcing is demonstrated

Corresponding author: Ranjini Swaminathan, r.swaminathan@reading.ac.uk

Abstract

Vegetation Gross Primary Productivity (GPP) is the single largest carbon flux of the terrestrial biosphere which, in turn, is responsible for sequestering 25–30% of anthropogenic carbon dioxide emissions. The ability to model GPP is therefore critical for calculating carbon budgets as well as understanding climate feedbacks. Earth System Models (ESMs) have the capability to simulate GPP but vary greatly in their individual estimates, resulting in large uncertainties. We describe a Machine Learning (ML) approach to investigate two key factors responsible for differences in simulated GPP quantities from ESMs: the relative importance of different atmospheric drivers and differences in the representation of land surface processes. We describe the different steps in the development of our interpretable Machine Learning (ML) framework including the choice of algorithms, parameter tuning, training and evaluation. Our results show that ESMs largely agree on the physical climate drivers responsible for GPP as seen in the literature, for instance drought variables in the Mediterranean region or radiation and temperature in the Arctic region. However differences do exist since models don't necessarily agree on which individual variable is most relevant for GPP. We also explore a distance measure to attribute GPP differences to climate influences versus process differences and provide examples for where our methods work (South Asia, Mediterranean) and where they are inconclusive (Eastern North America).

Plain Language Summary

Gross Primary Productivity (GPP) is the rate at which plants remove carbon dioxide from the atmosphere during photosynthesis. Carbon dioxide is a greenhouse gas and excess in the atmosphere causes global warming and climate change. Changes in the amounts of atmospheric carbon dioxide will impact the entire Earth System. We therefore need the ability to accurately calculate GPP, especially for different possible carbon usage pathways in the future. Earth System Models or ESMs allow us to simulate various processes happening in the earth's atmosphere and biosphere including photosynthesis and can help us estimate GPP changes for such different pathways. However, ESMs can vary significantly in their simulated GPP estimates making it difficult to have confidence in using these estimates. We describe a Machine Learning (ML) framework to better understand where ESMs differ in calculating GPP so that we can address knowledge gaps in models. This approach allows us to understand the processes involved without having to run computationally expensive simulations. With improved models, we can also improve our ability to predict climate change outcomes for the future.

1 Introduction

Terrestrial Gross Primary Production (GPP) is the flux of carbon into the land surface driven by photosynthesis.

It is estimated that terrestrial GPP is in the order of $\sim 132PgC$ and it is the single largest annual flux of the global carbon cycle. It plays a key role in determining atmospheric carbon dioxide, since approximately a quarter to a third of anthropogenic emissions are sequestered by the land surface (on Climate Change, 2023; Schimel et al., 2001; Schwalm et al., 2020). GPP is influenced by natural climate variability as well as anthropogenic factors associated with global warming (Santini et al., 2014; Zampieri et al., 2021). Our ability to estimate GPP, its spatio-temporal patterns and the factors influencing GPP is therefore essential to understanding and forecasting global carbon budgets with greater reliability. GPP is not a directly measurable quantity at spatial scales of interest for carbon budget calculations (global or regional), so we rely on indirect measurements with inevitable assumptions, for example about the partitioning of fluxes at eddy covariance

62 sites (Jung et al., 2019) or from satellite observations of quantities such as Solar Induced
63 Fluorescence (SIF) (Sun et al., 2017; Y. Zhang et al., 2018), which are not direct mea-
64 sures of the carbon flux.

65 Earth System Models (ESMs) provide the capability to simulate GPP by modelling
66 the various interactions between the atmosphere and biosphere including under differ-
67 ent climate change scenarios in the future (Fisher et al., 2018; Levis, 2010). However,
68 there is not only a large spread in GPP estimates from different ESMs but there are also
69 large uncertainties in observational products that could be used to evaluate these esti-
70 mates (Z. Wu et al., 2017; Anav et al., 2015). Therefore, there is a real need for eval-
71 uation methods that will help us understand better the possible reasons for such a large
72 spread in GPP simulations, both in terms of the influence of atmospheric variables driv-
73 ing GPP as well as in the representation of the processes involved in simulating GPP.
74 Identifying these differences can further help us address key gaps in modeling the ter-
75 restrial carbon cycle and will make for more reliable simulations from ESMs.

76 Machine Learning (ML) approaches have recently been used extensively in the study
77 as well as generation of more accurate GPP data sets. Examples are seen work done in
78 simulating GPP using observations of meteorological data or satellite data (Z. Zhang et
79 al., 2021; Sarkar et al., 2022), upscaling GPP estimates from eddy covariance sites (Yu
80 et al., 2021), to constrain uncertainty in GPP projections from models (Schlund et al.,
81 2020) and for evaluating GPP representation in models (Z. Zhang et al., 2021; Dunkl et
82 al., 2023). Our goal in this study is to use interpretable Machine Learning approaches
83 (Molnar, 2020; Doshi-Velez & Kim, 2017) to better understand the sources of differences
84 in GPP estimates between ESMs. Such an ML based evaluation framework can serve
85 as a basis for process based improvements to ESMs, complementary to existing strate-
86 gies, and can help reduce process uncertainty in modelled GPP estimates leading to more
87 reliable simulations.

88 In previous studies, differences in GPP estimates from ESMs have been attributed
89 to differences in the simulations of climate projections, modeling of complex terrestrial
90 processes such as dynamic vegetation modeling, as well as atmospheric CO_2 concentra-
91 tions for given emission scenarios (Nishina et al., 2015; Schwalm et al., 2020; Fisher &
92 Koven, 2020; Kim et al., 2018; Koch et al., 2021). In this work, we focus on two key at-
93 tributes responsible for variability in GPP across ESMs - (a) the differences in climate
94 simulations or input atmospheric forcing influencing GPP in individual models and (b)
95 differences arising from vegetation process representation in these models. While we ac-
96 knowledge that GPP is dependent on several land and atmospheric variables, in keep-
97 ing with other similar studies such as Churkina and Running (1998); Schwalm et al. (2020);
98 Anav et al. (2015), we evaluate the influence of three atmospheric variables as primary
99 determinants of photosynthesis – precipitation, air temperature and downwelling short-
100 wave radiation.

101 Our framework uses simulations from the CMIP pre-industrial Control (pi-Control)
102 experiments that simulate climate before industrialization and the addition of anthro-
103 pogenic CO_2 to the atmosphere. These simulations do not have the effects of elevated
104 CO_2 that could lead to vegetation feedbacks or of any warming signal due to climate change.
105 This allows us to better isolate the direct influence of the input climate variables on GPP
106 without these factors. ESM simulations from pi-Control runs are also run for longer time
107 periods, typically a few hundred years as opposed to a few decades from the historical
108 experiment simulations and so this gives us a larger data set to learn from.

109 The methods used in this framework are based on Information Theory and Machine
110 Learning, and compare the differences in input atmospheric forcings and vegetation pro-
111 cess modeling associated with simulating GPP, across different ESMs from the Sixth Phase
112 of the Coupled Model Intercomparison Project (CMIP6) (Eyring et al., 2016). These meth-
113 ods are directed towards formulating informed hypotheses for investigating the under-

114 lying factors influencing GPP estimates from ESMs. Specifically, the methods described
 115 target the following questions:

- 116 1. How do CMIP6 models differ in the input atmospheric forcings they consider most
 117 relevant for GPP? This will help us understand potential differences in how cli-
 118 mate variables may influence GPP across models.
- 119 2. Can we compare differences in input forcings across ESMs with their process based
 120 differences? This will guide us towards attributing differences in GPP to the ap-
 121 propriate underlying factors.

122 We address the above questions by building ML based emulators of CMIP6 mod-
 123 els that estimate GPP with input climate data. We query these emulators using robust
 124 Feature Selection methods to determine the relevance of individual atmospheric variables
 125 with respect to GPP. We also compare the differences in input forcing vs GPP by us-
 126 ing a distance metric called the Jensen-Shannon distance measure. This is a novel ap-
 127 proach that allows a comparison of two different attributory factors responsible for GPP
 128 and to the best of our knowledge is not previously seen in the literature.

129 We find that while the CMIP6 models considered largely agree on the variables con-
 130 sidered relevant for GPP, there are regions of uncertainty such as the tropics. We are
 131 also able to show that models with similar input forcings do not always show similar es-
 132 timates in GPP, indicating differences in process representation possibly due to param-
 133 eterization. The remainder of the paper is organized as follows – Section 2 describes the
 134 ML framework including the parameter tuning process and algorithmic description of
 135 the learning and Feature Selection approaches. In Section 3, we discuss results where the
 136 ML framework identifies differences in climate variables influencing GPP across ESMs.
 137 In Section 4, we discuss the interpretability of the ML framework described, how this
 138 framework can be used for evaluation and some of the challenges involved. Finally we
 139 present our conclusions and planned future work using for this framework in 5.

140 2 Data and Methods

141 2.1 Data and Pre-processing

142 Our experimental experimental input data consists of five ESMs (UKESM1-0-LL,
 143 IPSI-CM6A-LR, CanESM5, CNRM-ESM2-1 and GISS-E2-1-G) from the CMIP6 project,
 144 all with different vegetation and land surface models as shown in Table2.1. The crite-
 145 ria applied for selection was to pick a small set of models with diversity in their vege-
 146 tation modeling schemes, permitting exploration of various aspects of GPP simulation
 147 through our ML framework.

148 Seasonal means were calculated from monthly means of the data for two seasons,
 149 the boreal summer season of June-July-August (JJA) and austral summer season of December-
 150 January-February (DJF). All data considered is from the pre-industrial control (pi-Control)
 151 experiments which do not have an anthropogenic warming signal and for which a few
 152 hundred years of data are available from every model. Analysis is done for regions de-
 153 fined in the Intergovernmental Panel on Climate Change’s Sixth Assessment Report (IPCC
 154 AR6), (Gutiérrez et al., 2021). Data was downloaded and pre-processed from the Earth
 155 System Grid Federation servers (Cinquini et al., 2014) using the open source evaluation
 156 tool, ESMValTool (Righi et al., 2020). We removed all non-land grid cells of a model in
 157 a selected region to focus on terrestrial GPP and then sampled data uniformly across
 158 time and space. Every grid cell and every time instance constitutes a sample data point
 159 and for each data point, we have one value each for the three atmospheric variables as
 160 well as for GPP. We then use this pre-processed data for further analysis. A pictorial
 161 description of our ML framework is shown in Figure 1.

Earth System Model	Land Surface Model	Reference	Dynamic Vegetation
UKESM1-0-LL	Joint UK Land Environment Simulator (JULES)	(Sellar et al., 2019; Clark et al., 2011)	Yes
IPSL-CM6A-LR	Organising Carbon and Hydrology In Dynamic Ecosystems (ORCHIDEE)	(Boucher et al., 2020; Krinner et al., 2005)	No
CanESM5	The Canadian Land Surface Scheme (CLASS)	(Swart et al., 2019; Verseghy, 2012)	No
CNRM-ESM2-1	Interaction Soil-Biosphere-Atmosphere (ISBA)	(S��ferian et al., 2019; Delire et al., 2020)	No
GISS-E2-1-G	ENT Terrestrial Biosphere Model	(Kelley et al., 2020; Kiang, 2012)	No

Table 1. The CMIP6 models evaluated with our framework and their corresponding vegetation models. Data on dynamicity of vegetation obtained from the Earth System Documentation Project (Greenslade et al., 2014) and (Zarakas et al., 2020)

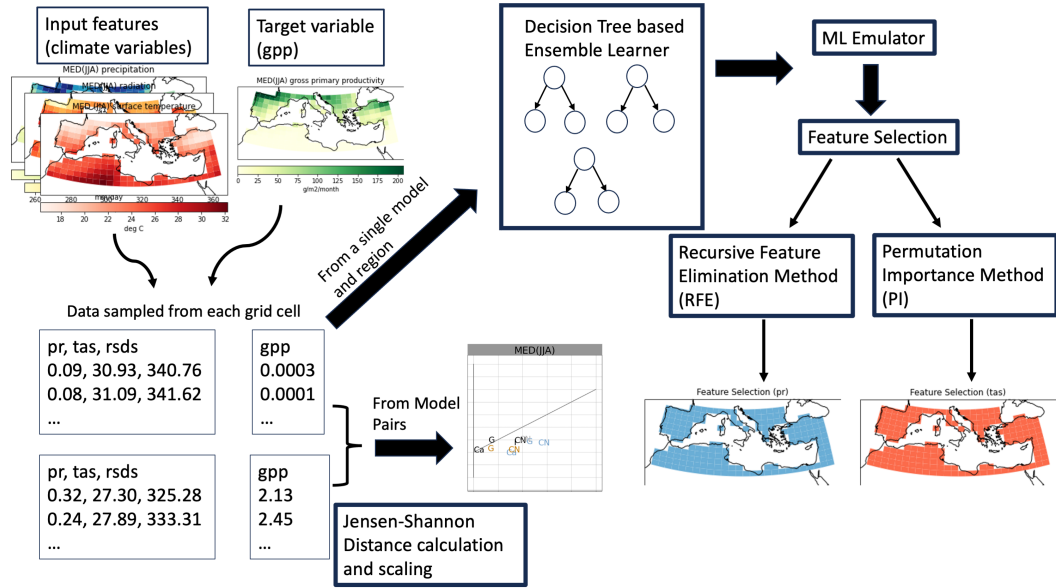


Figure 1. A description of the Machine Learning framework for evaluating GPP in CMIP6 models: Data from atmospheric variables and GPP for a given region, season and ESM is used to train an ensemble learner which serves as the ML emulator. The ML emulator is then queried using two different Feature Ranking algorithms (RFE or Recursive feature Elimination and PI or Permutation Importance) to find the most relevant features or atmospheric variables for GPP in that region. Data from pairs of ESMs is also used to calculate the Jensen-Shannon Distance (JSD) metric to compare distances measured in the input variable space with distances measured in the GPP distributions across regions.

162

2.2 ML Emulators with Ensemble Learning

163

164

165

166

167

168

169

170

171

172

173

174

175

176

177

178

179

180

181

182

183

184

185

186

187

188

189

190

191

192

193

194

195

Our requirement for an ML based emulator was one that would effectively model the relationship between input atmospheric forcing variables (and any other similar GPP influencing variables to be included as needed) and GPP; and one that would allow us to interpret or make inferences on the modeled relationships to answer questions on the relative importance or sensitivity to the climate variables. An additional goal was to develop a flexible framework that could be applied to observed data to better facilitate model evaluation. For this reason, we designed the core of the emulator to be a multivariate regression model and one that can be interpreted or queried on the decisions made for regression. In this, the climate forcing variables are the input features or predictors and GPP is the predictand. The ML emulator is trained for every region, season and ESM in our experimental setup. We use a regression model with Boosting called Adaptive Boosting or AdaBoost (Mendes-Moreira et al., 2012; Schapire, 2013) for our framework. Boosting is a well established ML approach that works towards developing a highly accurate prediction rule by repeatedly combining several weaker predictors or learners (Drucker, 1997) which in this case would be regressors. In Boosting, the first weak predictor is trained with a subset of samples uniformly sampled from the training data set with replacement permitted, meaning a training sample can be used again to build a different predictor. Once a predictor is built, all the training samples are passed through the predictor and the samples with the largest prediction errors are identified. The sampling probabilities of the samples with the most error are adjusted so that they are more likely to get picked as training samples for the next weak learner to be built. As this process repeats, harder to learn patterns get picked more often to build subsequent predictors. This means that some predictors will do better than others in a given subspace of the input feature space. The predictors are further assigned weights of the form, $\beta = \frac{\bar{L}}{1-\bar{L}}$ where \bar{L} is a calculated loss function. Cumulative predictions are calculated as a weighted median of all the predictors. The algorithm terminates when the average loss across all weak learners is below a certain threshold. The weak learners or regressors in this boosting algorithm can be any one of a wide array of regression methods. We calculated the Root Mean Square Error scores on held out test data sets and determined that the Decision Tree algorithm described in Breiman et al. (1984); Quinlan (1986); Breiman (1996) was best suited for our task after experimenting with different ML regression algorithms such as Linear Regression (James et al., 2021) and Support Vector Machines (Smola & Schölkopf, 2004). We therefore use an Ensemble Tree Learner with Boosting for our ML emulators.

196

197

198

199

200

201

202

203

204

As shown in Fig 1, CMIP6 data in the form of gridded data sets was used to train the ML emulators by treating each grid cell at every time step as an individual sample for learning. However, ESMs differ in grid resolution and in the length or number of years of the pi-Control experiment runs. So, for a given region, the number of training samples can be different across ESMs. In order to avoid biases resulting from differences in the number of samples, we randomly sampled a minimal sample set from every model such that the number of samples to train an emulator is the same across all ESMs. This sample set is then used to tune the parameters and build the Decision Trees in the ML emulator.

205

2.3 Parameter Tuning

206

207

208

209

210

211

212

213

In applied Machine Learning, parameter tuning is considered an important step in developing ML models that best capture patterns in the training data without overfitting (Yang & Shami, 2020). Overfitting occurs when we train the ML model to fit the training data too well which could result in a loss of generality. In other words, the ML model performs exceedingly well on the data it is trained with but fails to perform well on a new test set of samples even if from the same or similar distribution. We employ the Adaboost algorithm with an ensemble of Decision Tree regressors from the open source Python Scikit-learn package (Pedregosa et al., 2011) to build our ML emulators. A built

214 in mechanism for pruning the ensemble learner exists for removing learners in a way that
 215 diversity is maximized. This essentially means that learners are selected such that a wide
 216 range of associations or rules are learnt and duplication of rules learnt is minimized by
 217 pruning. This helps to avoid overfitting by balancing the need to add more rules in the
 218 predictor with the ability to generalize well. In our experiments we tune for the depth
 219 parameter in the Decision Tree for optimal performance of the emulator, determined as
 220 the best fit to the data as evaluated by the Root Mean Squared Error (RMSE) in the
 221 predictions. The depth of the Decision Tree is the number of levels at which decision nodes
 222 are split in the tree. For example, a decision could be $tas > 20$ which would split train-
 223 ing samples into those where the surface temperature is greater than 20°C (condition
 224 is true) and those where the temperature is less than 20°C (condition is false) and so
 225 on. For every region-season-ESM combination, we split the samples available into a train-
 226 ing set and a held out test set. The ML emulator (AdaBoost with Decision Tree regres-
 227 sor) is learnt using the training samples and tested on the held out samples. RMSE scores
 228 are calculated for both training and held out test sets. For a given value of the depth
 229 parameter, this process is repeated by splitting the data n times and the average train-
 230 ing and test RMSE scores over the n splits is calculated. This is how n -fold cross-validation
 231 (where $n=6$ in this case) is performed. The depth parameter that has the lowest RMSE
 232 score on the held out test data, with cross-validation is then chosen as the most opti-
 233 mal parameter for the task and a final ML emulator is built using that depth param-
 234 eter and all the samples available for that region. This builds robustness against overfit-
 235 ting, and sampling multiple times during cross validation further makes the model more
 236 reliable ensuring that the final emulator has seen a good representation of the available
 237 data. ML emulator estimates of GPP for a selection of regions are shown as an illustra-
 238 tion of the results from this process in Supplementary Figure S1.

239 2.4 Feature Selection Methods

240 After the ML emulators were constructed to specification and sufficiently satisfied
 241 requirements, meaning the final emulator had the lowest possible RMSE scores for held
 242 out test data in cross validation experiments as described, we focused on querying or in-
 243 terpreting these emulators to better understand the relationship between the different
 244 input climate variables and GPP. Feature Selection or Feature Importance Ranking is
 245 the process of selecting or ranking features (input variables or predictors) that are most
 246 relevant to the predictand as evaluated by some chosen measurement or metric (Kumar
 247 & Minz, 2014; Guyon & Elisseeff, 2003). It is a process that is often used to prune the
 248 number of input features required for accurate predictions but in our case, with just three
 249 features, we use feature ranks to find the input atmospheric forcing variable(s) that the
 250 ML emulators find most important for GPP. Two different feature selection methods were
 251 applied to the ML emulators - (a) Recursive Feature Elimination (RFE) and (b) Per-
 252 mutation Importance (PI). The two methods use slightly different criteria to evaluate
 253 feature importances as described below but both provide useful information regarding
 254 the relative importance of a climate variable for GPP and are complementary. In the Re-
 255 cursive Feature Elimination algorithm, the input features are recursively removed one
 256 at a time to find the feature that has the most influence on the predictand (Guyon et
 257 al., 2002). For our experiments, we used the RMSE values to quantify the influence of
 258 an input climate variable on GPP. So, if the RFE method determines precipitation to
 259 be the most important feature for GPP, this effectively means that removing precipita-
 260 tion from the set of input features would have the most impact on the emulator's abil-
 261 ity to predict GPP well i.e increase the RMSE by the most compared to other variables.
 262 In the Permutation Importance method, the decrease in model score when an individ-
 263 ual feature is randomly shuffled or permuted is the measure of how important that fea-
 264 ture is to the emulator (Breiman, 2001). The model score here is the Regression coef-
 265 ficient of determination (R^2) and is a measure of how well the ML emulator fits the data.
 266 Thus, the PI method works well once a reliable ML emulator is developed and is a mea-

267 sure of sensitivity of GPP to an input variable given such an emulator. As in the case
 268 of developing the ML emulator, we performed 6-fold cross-validation for the feature se-
 269 lection process as well. We did this by devising a simple voting scheme with small dif-
 270 ferences based on the Feature Selection approach. In the case of the RFE method, we
 271 assigned a single vote to the feature(s) that was ranked highest in terms of influencing
 272 the prediction with the RMSE score. We then averaged the votes across all the input
 273 features to determine the actual ranks of these features. In the PI method, we calculated
 274 the contribution of each feature to the R^2 score (permutation importances) and granted
 275 a vote to an input feature if it contributed to more than half of the score, which is the
 276 fit of the model. As in the RFE method, the votes were once again averaged across the
 277 cross-validation subsets. This scheme allowed us to account for collinearity or multiple
 278 variables equally influencing GPP especially as these are physical climate variables which
 279 are very closely related to each other.

280 2.5 Distance measure for climate and GPP distribution comparisons

281 While the ML emulators and Feature Selection are used to understand differences
 282 in models, we also calculate using a relative measure, how close or similar models are in
 283 the input forcing space vs. how similar they are in their simulated GPP distributions.
 284 Essentially we evaluate whether models that are similar in input atmospheric forcing sim-
 285 ulated by the ESMs are also similar in their GPP simulations. If we consider that ev-
 286 ery data sample is represented as an instance in a 3-Dimensional input climate param-
 287 eter space, where each dimension corresponds to a climate feature, then for a given region-
 288 season-ESM, we have a distribution of these 3-Dimensional data points. A distance met-
 289 ric is applied to quantify how close climate distributions from two different ESMs are
 290 for a given region and season. The same distance metric is now used to measure simi-
 291 larity between the GPP distributions of models in the 1-Dimensional space of GPP val-
 292 ues. The distance metric we use is the Jensen-Shannon distance, which is calculated as
 293 the square root of the Jensen-Shannon divergence between two distributions (Lin, 1991).
 294 This is a symmetric and smoothed version of the more commonly used Kullback-Divergence
 295 measure. This measure has been widely used in applications such as evaluating gener-
 296 ative adversarial networks by measuring differences in distributions (Goodfellow et al.,
 297 2020), text classification with high dimensional feature sets (Dhillon et al., 2003) and
 298 in bioinformatics for mutation detection (Gültas et al., 2014). The Jensen Shannon Di-
 299 vergence itself is defined as :

$$JSD(P\|Q) = \frac{1}{2}D(P\|M) + \frac{1}{2}D(Q\|M), M = \frac{1}{2}(P + Q), \quad (1)$$

300 where $D(P\|Q)$ is the Kullback-Divergence (Csiszár, 1975) between two distributions P
 301 and Q. When a base-2 logarithm is used, the Jensen-Shannon divergence has an upper
 302 bound of 1 i.e, $0 \leq JSD(P\|Q) \leq 1$. The existence of upper and lower bounds and
 303 the fact that distances are symmetric, are important properties we take advantage of when
 304 comparing ESMs. We refer to JSD as the Jensen-Shannon Distance instead of divergence
 305 as they both hold the same meaning for our analysis. Using the JSD, we compare how
 306 much ESMs differ in their input forcing vs in the simulated GPP for a region and sea-
 307 son. A JSD of 0 implies the distributions are identical and as the JSD increases going
 308 towards 1, it implies that distributions get more dissimilar. While it is not possible to
 309 directly compare distance values between pairs of ESMs across two different distribu-
 310 tion spaces (as in the 3-D climate space and the 1-D GPP space), we can compare how
 311 ESM-pair distances are ordered in both distribution spaces. That is we can see how dis-
 312 tances between pairs of models compare in the two different spaces. We further apply
 313 a simple scaling by a factor of the shortest distance among all pairs of models in the in-

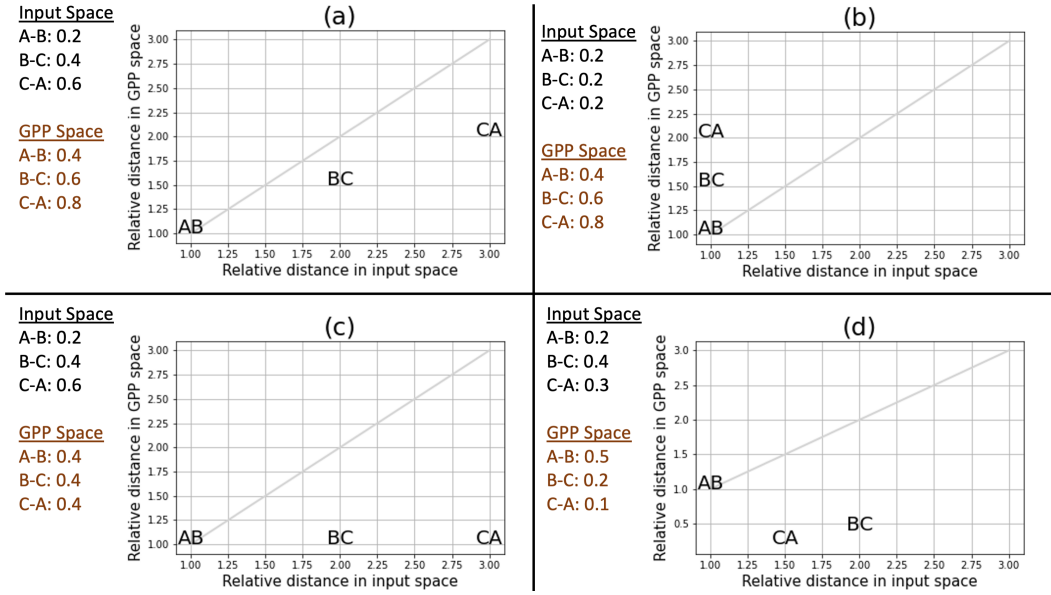


Figure 2. An illustration of how the Jensen Shannon distance metric is used to understand differences in input space (atmospheric forcings) and GPP space. In subplot (a) of the figure, we can make the inference that similarities in input forcing are consistent with similarities in GPP. Where that does not hold, we can start to explore the possibility that there might be larger differences in process representation or parameterization between pairs of ESMs which results in this difference in GPP as seen in subplots (b) and (c) and in the case of model pair A-B in (d). Thus the JSD scaled in this manner gives us a way to actually compare the differences in input forcings of ESMs relative to their simulated GPP.

314
315

put space so we can effectively make inferences about whether relative orderings in input climate variable space are reflected in the GPP space as well.

316
317
318
319
320
321
322
323
324
325
326
327
328
329
330
331
332
333
334
335
336

We illustrate analysis based on the JSD in Figure 2 with four different possible use cases and how inferences can be made from them. Each sub figure shows the actual JSD in input (on the x-axis) and GPP (y-axis) space between three hypothetical models - A, B and C. The distances are then scaled by dividing all the distances in input space by the smallest such distance among all pairs of models. The distance in GPP space between that same pair of models is then used to scale all model pair distances in GPP space. This scaling allows us to effectively compare distances in input space vs GPP space. In subplot (a), we see that the relative ordering of distances between pairs of models is the same on both axes, the model pair A-B has the smallest distance in input space as well as GPP space while the model pair C-A has the largest distance in both these spaces. This provides some evidence that similarities or differences between pairs of models in the atmospheric forcing is also reflected in their GPP simulations. In (b), the distances in the atmospheric forcing are the same for all pairs of models but that's not the case in their GPP simulations where the distance between C-A is larger than the other pairs indicating possible differences in process representation across the models. In (c), the model pairs show larger differences in their input forcing but not in the simulated GPP space, indicating that despite having different climate, the models end up simulating very similar GPP values potentially differing in the processes involved in calculating GPP from these climate variables. Finally, in (d) we see another example for where proximity in input forcing does not translate to similar GPP simulations. In model pair A-B, differences lie more in simulated GPP than in the atmospheric forcing while the opposite is

337 the case for model pairs C-A and B-C. We can thus use this analysis to attribute rea-
 338 sons for differences in GPP simulations between pairs of models.

339 The JSD measure was also used to determine how well the ML emulators estimate
 340 GPP by comparing the emulator estimated values with ESM simulations and we found
 341 that these distances tended to zero (results not shown). This further gives us confidence
 342 in our deployment of these ML emulators.

343 The ML emulators with Feature Selection, Jensen-Shannon Distance metric com-
 344 parisons and more traditional analysis involving univariate statistics are all combined
 345 in our analysis of differences across ESMs in how they simulate GPP. Results from the
 346 analysis and a discussion on where the ML methods work well and where they don't is
 347 discussed in the next sections.

348 **3 Results**

349 In this section, we look at two key sets of results coming from the ML framework
 350 proposed in section 2.4. We first look at regional feature importances, that is, what the
 351 ML emulators determine to be the most relevant climate variable for GPP in a given re-
 352 gion. We discuss results for regions in the JJA and DJF seasons as seen in Figures 3 and
 353 4 but also provide results from the annual mean analysis for a more general overview in
 354 Supplementary Figure S2. We study the differences and similarities in GPP represen-
 355 tation across pi-Control simulations in ESMs but due to the lack of observational datasets
 356 for this period, we use the literature on historical observations to guide our evaluation.

357 Our second set of results is from the comparison of relative distances between ESMs
 358 in the input climate space vs the GPP distribution space as described in Subsection 2.5
 359 and shown in Figure 5. In our current analysis, we provide examples for how the JSD
 360 based comparisons can be useful as a tool to identify potential sources of differences in
 361 ESMs but leave more detailed region by region analysis for future work.

362 **3.1 Model differences in relevant climate variables for GPP**

363 Figures 3 and 4 show the most relevant climate variables for predicting GPP from
 364 two feature selection methods – Recursive Feature Elimination (RFE) and Permutation
 365 Importance (PI) in the first and second columns respectively. The RFE method's selec-
 366 tion of best feature is considered the most relevant variable for GPP by the ML emu-
 367 lator and means that this variable is primarily responsible for estimating GPP. The PI
 368 method's selection on the other hand is more a measure of GPP's sensitivity to climate
 369 variables given the ML emulator. The most important climate variable could also be the
 370 variable GPP is most sensitive to, as in both methods could agree on the choice of cli-
 371 mate variable(s) but differences are possible since the metrics involved are slightly dif-
 372 ferent (low error vs best fit). ESM differences in the top features from the methods are
 373 considered an appropriate potential starting point for investigating divergence in GPP
 374 estimates from ESMs. We refer to the regions by their acronyms as defined in Iturbide
 375 et al. (2022) and are shown in Supplementary Figure S3 for reference.

376 Overall, all ESMs considered agree that temperature followed by precipitation are
 377 key variables for GPP for most of Europe, N.America and Asia. Over Africa and S.America,
 378 there is less of a consensus across ESMs and methods in accordance with previous anal-
 379 ysis (Churkina & Running, 1998). Temperature is considered the most important vari-
 380 able for GPP in the Russian-Arctic (RAR) and Northern Europe (NEU) regions in JJA
 381 for most ESMs. Conditions of almost constant sunlight and water availability make tem-
 382 perature the key driver for GPP here. The northern N.American regions are a combi-
 383 nation of arctic tundra and boreal forests and similarly show temperature as the main

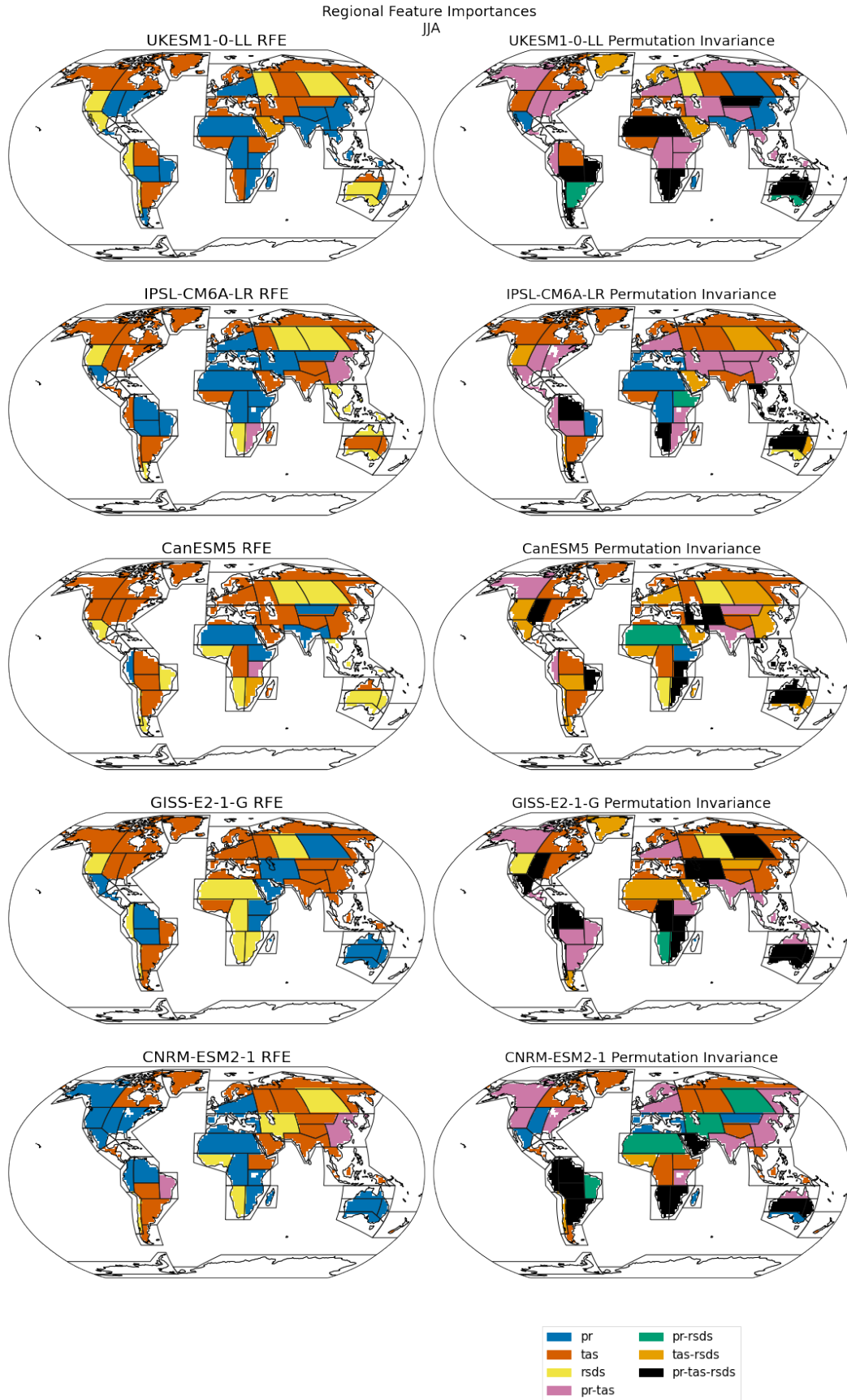


Figure 3. JJA feature importance from two methods - Recursive Feature elimination and Permutation Invariance for the IPCC regions defined in Iturbide et al. (2022).

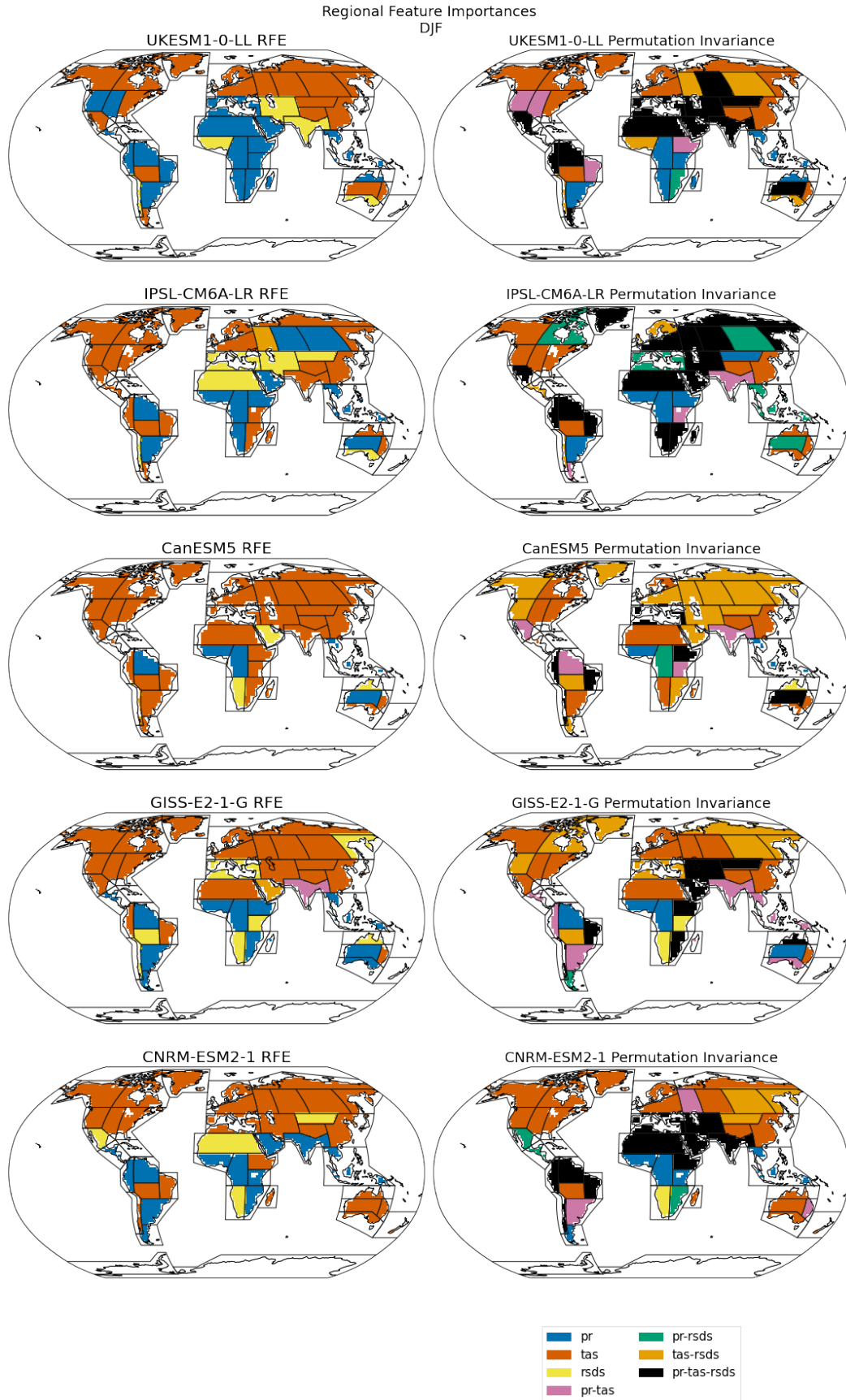


Figure 4. DJF feature importance from two methods - Recursive Feature elimination and Permutation Invariance for IPCC regions defined in Iturbide et al. (2022)

384 driving factor except for Northwestern North America (NWN) in CNRM-ESM2-1 where
385 precipitation is determined as the key driver.

386 Boreal forest regions such as Eastern Europe (EEU), Western and Eastern Siberia
387 (WSB, ESB) and the Russian Far East (RFE) show more divergence across ESMs with
388 GPP being more dependent in both RFE and PI methods on temperature or radiation
389 or both but in some instances (ESB for GISS-E2-1-G) on precipitation. In the central
390 and eastern continental United States (CNA, ENA), UKESM1-0-LL and CNRM-ESM2-
391 1 models consider precipitation to be most relevant for GPP while all other models find
392 temperature more relevant. The variability in GPP is also dominated by a combination
393 of these two variables as seen in the PI method. In the western north American region
394 (WNA), radiation is seen as driving GPP except in CanESM5 (temperature) and CNRM-
395 ESM2-1 (precipitation). In fact, precipitation seems to be most relevant for GPP in al-
396 most all N.American regions in the CNRM-ESM2-1 model and this can be considered
397 as an indication that either the availability or the parameterization of this variable is im-
398 portant for GPP in this model more so than in others.

399 All ESMs in our study agree precipitation and temperature play a more important
400 role than radiation in the Mediterranean region (MED), where radiation is largely avail-
401 able and a lack of rainfall or very high temperature is likely to influence vegetation more
402 (Gea-Izquierdo et al., 2015). The CNRM1-ESM2-1 and IPSL-CM6A-LR are the two mod-
403 els that rank precipitation higher than temperature as an important feature. For the re-
404 gion covering the Indian subcontinent (SAS), precipitation is considered most important
405 in the UKESM1-0-LL and CanESM5 models, consistent with previous studies (Varghese
406 & Behera, 2019; Verma et al., 2022) while all three other models favor temperature as
407 the key factor. In East Asia (EAS) temperature is considered the most important driver
408 for GPP followed by precipitation and radiation in some regions (Yao et al., 2018; Bo
409 et al., 2022) and all models except UKESM1-0-LL (precipitation) are in agreement.

410 In the DJF season, all models except CanESM5 consider precipitation most rel-
411 evant for GPP in South East South America (SES) and all models agree that temper-
412 ature is most relevant for Eastern Australia (EAU). We find the largest source of dis-
413 agreement with regards to GPP drivers (looking at both DJF and JJA seasons) in re-
414 gions where there is a significant presence of tropical forests such as Northern South Amer-
415 ica (NSA), Central-Africa (CAF), South-East Asia (SEA) and Northern Australia (NAU).
416 We note radiation plays a role in some regions, possibly due to the lack of sufficient ra-
417 diative energy available due to cloud cover which makes it hard to distinguish the rel-
418 ative importance between features. However almost all ESMs over a majority of these
419 regions reference temperature and precipitation as key variables and from observational
420 records we know that the two variables are strongly correlated in these regions (Nzabarinda
421 et al., 2021; F. Zhang et al., 2022; Kanniah et al., 2011). Although precipitation appears
422 most frequently as the most important variable in determining GPP, especially us-
423 ing the RFE method of feature selection, in more than one instance all three features
424 are considered relevant. This is consistent with results from previous studies using ob-
425 servations and non-ML approaches applied to finding GPP drivers (Churkina & Run-
426 ning, 1998; Kanniah et al., 2013; D. Wu et al., 2014). Another area where models lack
427 consensus over the drivers is Southern Africa (ESAF and WSAF) for the DJF season.
428 In reality, these areas are dominated by savannah, and are likely water limited but this
429 is seen only in the UKESM1-0-LL model. Water limitaion effects on GPP in ESMs is
430 typically modelled quite crudely, with uncertain parameterization (Harper et al., 2020)
431 , and this is likely a significant source of disparity between the models.

432 3.2 Comparing differences in climate forcing vs GPP in model pairs

433 We compare ESM differences in the input feature space with their GPP distribu-
434 tions with the approach described in 2.5. In Figure 5 we show the comparative distances

435 as a scatter plot to illustrate how we can potentially develop our hypotheses for quan-
 436 tifying and thus attributing differences in GPP to differences in climate forcing or pro-
 437 cess representation.

438 From the scatter plots in 5, we see differences across regions in how the pairwise
 439 model distances relate. If distances in input climate space between pairs of models trans-
 440 lated to similar distances in GPP distributions, we would see the data points scattered
 441 along the diagonal unit slope line as seen in the NSA region. However this is not always
 442 the case, and we see more of a spread along the input space or x-axis (MED, RAR and
 443 somewhat also in SAS) where the plot indicates a spread in climate not quite seen in the
 444 simulated GPP and where relative differences in GPP are smaller than in input forcing
 445 . In other regions (SEA) however almost all pairs are above the unit slope line, which
 446 means that distances are larger in the GPP space.

447 We can use information from where there is a spread to investigate the likely causes
 448 underlying GPP divergence across models. In at least two regions (RAR and SAS), we
 449 notice that relative model distances with UKESM1-0-LL are greater in the y-axis even
 450 though such distances in the input space lie more or less in the middle range. This is an
 451 indication that the GPP simulated by UKESM1-0-LL is most different compared to other
 452 models even though not largely different in climate. In the SAS region for instance, the
 453 IPSL-CM6A-LR and UKESM1-0-LL models are closest in input space relative to other
 454 model pairs (seen as black colored letter I), and the CanESM5 model is identically dis-
 455 tanced from both these models in the input space (seen as black and blue letters Ca).
 456 However, we see that in GPP space the UKESM1-0-LL distance with CanESM5 is more
 457 than the distance between CanESM5 and IPSL-CM6A-LR. Therefore one hypothesis worth
 458 investigating for this region is whether GPP process representation in IPSL-CM6A-LR
 459 and CanESM5 is similar in parameterization and different from UKESM1-0-LL. We would
 460 also include information from our feature importance results in 3 where we see that the
 461 two models differ in the variable considered most relevant for GPP (this is precipitation
 462 for UKESM1-0-LL, CanESM5 and temperature for IPSL-CM6A-LR). We argue that this
 463 type of analysis would be difficult to apply if we only consider univariate statistics as we
 464 show with examples in Supplementary Figure S4.

465 As a counter example, the ENA and to some extent the WSAF regions are exam-
 466 ples of where it is not so clear how much of the difference in GPP to attribute to the in-
 467 fluence of atmospheric forcing vs process representation from the scatter plot in Figure
 468 5 due to close clustering in the relative distances.

469 4 Discussion

470 4.1 Choice of ML Approach for Evaluation

471 GPP is the largest individual carbon flux in the Earth System and changes to it
 472 have implications for the atmospheric carbon dioxide concentration, net carbon balance
 473 of the land surface and climate feedbacks (Friedlingstein et al., 2014). Interannual vari-
 474 ability in GPP is influenced by changes in climate especially in hotspot regions such as
 475 tropical forests (O’Sullivan et al., 2020; Jung et al., 2011). Earth System Models pro-
 476 vide the capability to simulate the Earth System’s biogeochemical interactions and car-
 477 bon cycle but global GPP estimates from ESMs vary greatly. For instance, in the five
 478 CMIP6 ESMs in our study, we found the global mean annual GPP to be in the range
 479 of 82-115 PgC year⁻¹ for the pre-industrial period. The need to evaluate the carbon cy-
 480 cle in ESMs is thus critical for both better process representation and for modeling in-
 481 teractions with other components of the Earth System such as the atmosphere (Spafford
 482 & MacDougall, 2021; Reichler & Kim, 2008). Advances in Machine Learning and AI
 483 provides the algorithms that can help to facilitate evaluation of these complex interactions
 484 and uncover process based differences across ESMs (Huntingford et al., 2019). Our ap-

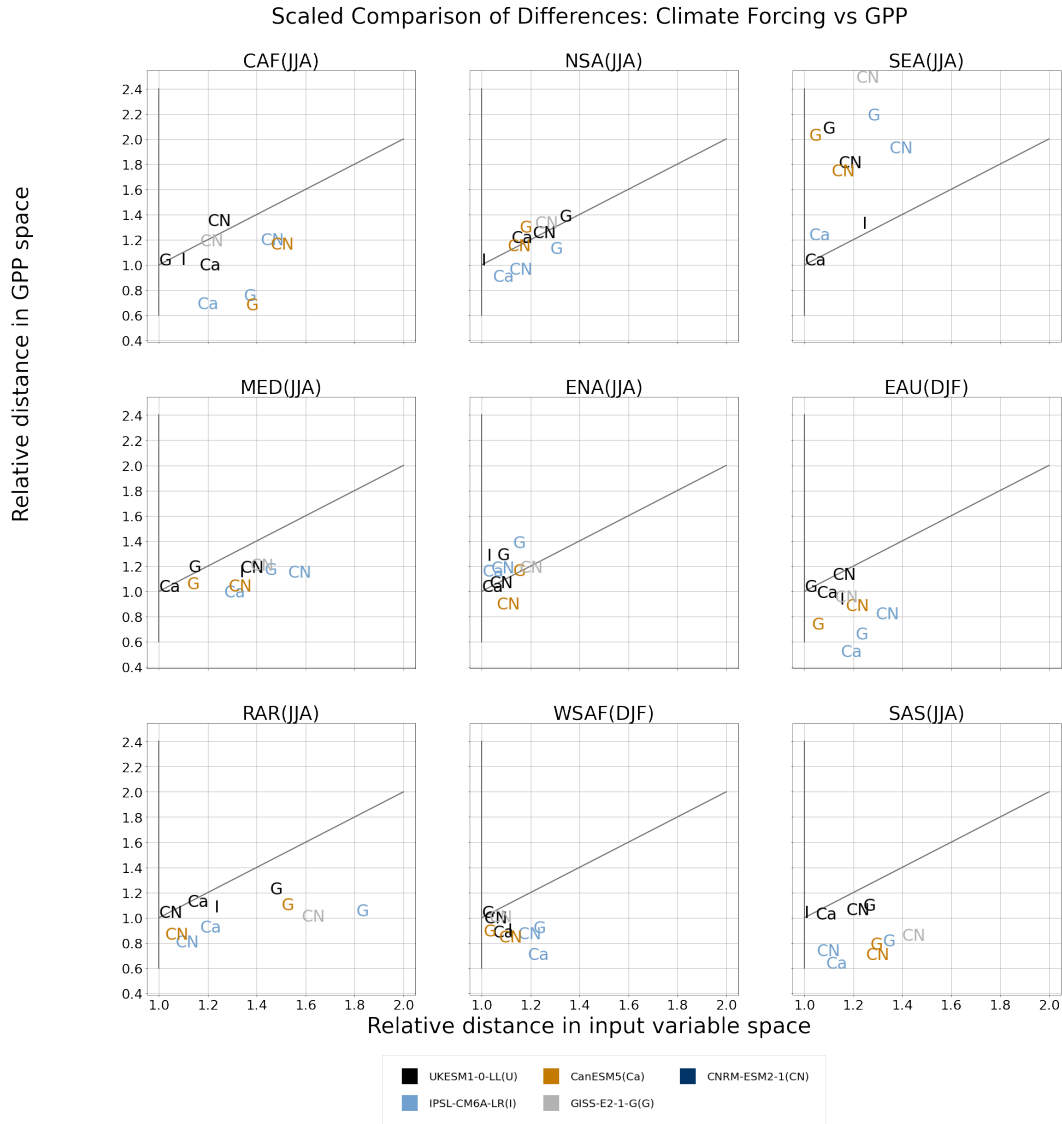


Figure 5. A comparison of relative distances in climate forcing and in GPP from different climate models is shown. Every model is referenced by both a color and an alphabet, the color and alphabet pairing tells us which pair of models are represented. Since the JSD is symmetric, there is only one colored symbol to show the distance between every pair of models. For this reason, there is no letter seen for the first model in the list, UKESM1-0-LL but its color (black) and letters for other models show the distance between UKESM1-0-LL and other models. For each region, the actual JSD values are scaled by factor that is the smallest distance in the input space across all pairs of models as seen in the x-axis and by the distance measure for that same pair in the GPP space as seen in the y-axis. This scaling follows from the description in Section 2 and Figure 2.

485 proach has been to start with the simplest ML models suited for our purpose. For this
 486 study, we build ML emulators with three input climate features to estimate GPP and
 487 for that emulator to be interpretable, which we demonstrate with our Feature Selection
 488 algorithms. Therefore, our ML emulators are not black boxes but can be interpreted in
 489 the context of physical and biogeochemical Earth System processes. We evaluated a choice
 490 of regression schemes before determining that Decision Trees best suited our task and
 491 further added better generalization capabilities with Boosting in the form of an Ensemble
 492 Learner with Adaboost. Such an emulator was capable of readily providing explanations
 493 on the modeled interactions between the atmospheric variables and GPP. At the
 494 same time, our framework is flexible enough for this emulator to be replaced with more
 495 complex ML algorithms such as Deep Architectures (LeCun et al., 2015) as we expand
 496 our suite of interacting variables for more nuanced evaluation of the carbon cycle. We
 497 further built robustness into our methods through rigorous cross validation and through
 498 the approaches outlined in Section 2.3 and demonstrate a reliable and adaptable frame-
 499 work that is also interpretable. With this framework, we were able to show regional sim-
 500 ilarities and differences in ESMs in the influence of key climate variables for GPP. Our
 501 emulator has the capability to capture non-linear relationships between the climate vari-
 502 ables and GPP which can help to address limitations or complement more traditional
 503 approaches using correlations or calculated indices seen in the literature (O’Sullivan et
 504 al., 2020; Seddon et al., 2016).

505 The second component of our framework is a way to compare differences in climate
 506 variables influencing GPP with differences in processes estimating GPP in ESMs and
 507 we choose an algorithm based on the Jensen Shannon distance that is robust against small
 508 variations in distributions, allows a comparison of the joint input space with three vari-
 509 ables and has bounds [0,1] to enable relative placement of distances. Also where a statis-
 510 tic such as a mean could be close for two different distributions, such as unimodal vs bi-
 511 modal, the JSD will capture a difference in parameterization resulting in quite different
 512 distributions with similar means. Finally, our method enables a more flexible and less
 513 expensive way to perform this comparison where previously modeling experiments had
 514 to be conducted for similar analysis (Hardouin et al., 2022).

515 4.2 Application of ML framework for GPP Evaluation

516 The ML framework described in this paper can be used to identify areas of differ-
 517 ences in GPP modeling in ESMs. For instance, from Figure 4 and Figure 3, we see that
 518 while models have overall agreement on what variables are important for certain regions
 519 (temperature and precipitation for the Mediterranean, South Asia, Eastern and Central
 520 North America; temperature and radiation in the tundra and boreal forest regions) dif-
 521 ferences exist in the which individual climate variable matters for a given ESM. Further
 522 the comparison using JSD gives us a starting point for whether these differences are more
 523 in the state of the climate influencing GPP or in the processing of these variables such
 524 as through parameterizations. This ML framework can serve as a guide to investigate
 525 probable reasons why differences in GPP modeling exist in ESMs in a computationally
 526 less expensive manner to actually running model simulations.

527 4.3 Limitations and Challenges

528 In our current study, we sample data uniformly from the spatio-temporal domain
 529 which does not capture sub-regional and sub-seasonal variability and trends. This lim-
 530 itation is mainly driven by the lack of availability of GPP data from CMIP6 ESMs at
 531 higher temporal resolutions for the pi-Control experiment. However, this is more a fea-
 532 ture of the data used and our framework will allow us to experiment with different res-
 533 olutions in data when available. The JSD approach provides a relatively inexpensive method,
 534 without actually having to run model simulations, to compare differences across mod-
 535 els in GPP vs climate variables but in some regions such as Eastern North America (ENA)

536 seen in Figure 5, it is harder to infer where the differences lie. Along with future work
 537 to develop this analysis, we also suggest that individual components of the ML frame-
 538 work as well as more traditionally considered descriptive statistics such as means and
 539 variability should all be used in a complementary fashion in the evaluation process so
 540 we can take insights from different modes of analysis. Finally, the three predictor vari-
 541 ables were chosen because of their importance in determining the supply of water (pre-
 542 cipitation), its loss through evapotranspiration (temperature) and the available energy
 543 for photosynthesis (shortwave radiation). We recognize the need to include a broader suite
 544 of variables for a more holistic evaluation of the carbon cycle which is possible to do with
 545 our framework.

546 5 Conclusions

547 This study demonstrates the potential of using interpretable ML approaches to in-
 548 vestigate differences in GPP modeling across a selection of CMIP6 models and over land
 549 regions defined in the IPCC's Sixth Assessment Report and two seasons. In conclusion:

- 550 1. The relative importance of key climate drivers for GPP was identified across dif-
 551 ferent regions and ESMs using Feature Selection Methods with interpretable ML
 552 emulators. We illustrate this with examples such as the Mediterranean region where
 553 all models agree that drought variables such as temperature or precipitation in-
 554 fluence GPP more than radiation but models differ in which of the two variables
 555 is most relevant.
- 556 2. With a comparative distance metric based on the Jensen Shannon Distance, we
 557 are able to show that proximity or distance in climate between any two models
 558 does not necessarily translate to a similar proximity or distance in their estimated
 559 GPP distributions with the Russian Arctic (RAR) and Mediterranean regions (MED)
 560 as two such examples. We take this as evidence that process based differences ex-
 561 ist across models and are at least partly responsible for differences in GPP esti-
 562 mates from ESMs.
- 563 3. Where the JSD method suggests divergence in GPP potentially due to process mod-
 564 eling, for instance in South Asia (SAS) between the UKESM1-0-LL, IPSL-CM6A-
 565 LR and CanESM5 models, the Feature Selection process can offer an explanation.
 566 In this case the UKESM1-0-LL and IPSL-CM6A-LR models differ in the key cli-
 567 mate variable for GPP but the UKESM1-0-LL and CanESM5 models don't and
 568 a possible reason for this can be differences in parameterization or characteristics
 569 of this variable not considered in the input features.
- 570 4. There are some regions where models do not show a clear consensus on what cli-
 571 mate variables matter the most or identify all three variables as equally impor-
 572 tant such as the tropics. Similarly our distance metric based comparison also presents
 573 cases where a direct inference on attributing GPP differences cannot be made, such
 574 as the Eastern North American (ENA) region. We identify these as regions of un-
 575 certainty to address in future work.

576 Data from the pre-industrial Control experiments served as a baseline for the develop-
 577 ment of this evaluation framework. In future work, additional climate drivers and char-
 578 acteristics such as sub-monthly variability will also be incorporated as possible causes
 579 for variations in GPP estimates from ESMs and analysis will be conducted with data
 580 from historical experiments and observations towards the goal of improving vegetation
 581 modeling in Earth System Models.

582 6 Open Research

583 Data from CMIP6 climate models is available for download on Earth System Grid
 584 Federation nodes and were downloaded and preprocessed using the open source software

585 ESMValTool v2.8.0 (doi:10.5281/zenodo.3401363) and ESMValCore v2.8.0 (doi:10.5281/zenodo.3387139).
 586 Code used to produce the results in this paper is available under the CC-BY license at
 587 the Github repository (<https://github.com/rswamina/gpp-ml-eval-1-publish>) which is
 588 currently private but will be made public once the manuscript has been accepted for pub-
 589 lication.

590 Acknowledgments

591 RS and TQ are funded by the UK Research Infrastructure Natural Environment Research
 592 Council (UKRI-NERC) funded TerraFIRMA: Future Impacts, Risks and Mitigation Ac-
 593 tions in a changing Earth system grant (NE/W004895/1). RA is funded by the National
 594 Centre for Earth Observation grant: NE/RO16518/1.

595 References

- 596 Anav, A., Friedlingstein, P., Beer, C., Ciais, P., Harper, A., Jones, C., ... others
 597 (2015). Spatiotemporal patterns of terrestrial gross primary production: A
 598 review. *Reviews of Geophysics*, *53*(3), 785–818. doi: 10.1002/2015RG000483
- 599 Bo, Y., Li, X., Liu, K., Wang, S., Zhang, H., Gao, X., & Zhang, X. (2022). Three
 600 decades of gross primary production (gpp) in china: Variations, trends, at-
 601 tributions, and prediction inferred from multiple datasets and time series
 602 modeling. *Remote Sensing*, *14*(11), 2564. doi: 10.3390/rs14112564
- 603 Boucher, O., Servonnat, J., Albright, A. L., Aumont, O., Balkanski, Y., Bas-
 604 trikov, V., ... others (2020). Presentation and evaluation of the ipsl-cm6a-
 605 lr climate model. *Journal of Advances in Modeling Earth Systems*, *12*(7),
 606 e2019MS002010. doi: 10.1029/2019MS002010
- 607 Breiman, L. (1996). Bagging predictors. *Machine learning*, *24*, 123–140. doi: /10
 608 .1007/BF00058655
- 609 Breiman, L. (2001). Random forests. *Machine learning*, *45*, 5–32. doi: doi.org/10
 610 .1023/A:1010933404324
- 611 Breiman, L., Friedman, J., Olshen, R., & Stone, C. (1984). Cart. *Classification and*
 612 *regression trees*.
- 613 Churkina, G., & Running, S. W. (1998). Contrasting climatic controls on the es-
 614 timated productivity of global terrestrial biomes. *Ecosystems*, *1*(2), 206–215.
 615 doi: 10.1007/s100219900016
- 616 Cinquini, L., Crichton, D., Mattmann, C., Harney, J., Shipman, G., Wang, F., ...
 617 others (2014). The earth system grid federation: An open infrastructure for
 618 access to distributed geospatial data. *Future Generation Computer Systems*,
 619 *36*, 400–417. doi: 10.1016/j.future.2013.07.002
- 620 Clark, D., Mercado, L., Sitch, S., Jones, C., Gedney, N., Best, M., ... others (2011).
 621 The joint uk land environment simulator (jules), model description–part 2:
 622 carbon fluxes and vegetation dynamics. *Geoscientific Model Development*,
 623 *4*(3), 701–722. doi: 10.5194/gmd-4-701-2011
- 624 Csiszár, I. (1975). I-divergence geometry of probability distributions and mini-
 625 mization problems. *The annals of probability*, 146–158. doi: 0.1214/aop/
 626 1176996454
- 627 Delire, C., Séférian, R., Decharme, B., Alkama, R., Calvet, J.-C., Carrer, D., ...
 628 others (2020). The global land carbon cycle simulated with isba-ctrip: Im-
 629 provements over the last decade. *Journal of Advances in Modeling Earth*
 630 *Systems*, *12*(9), e2019MS001886. doi: 10.1029/2019MS001886
- 631 Dhillon, I. S., Mallela, S., & Kumar, R. (2003). A divisive information theoretic fea-
 632 ture clustering algorithm for text classification. *The Journal of machine learn-*
 633 *ing research*, *3*, 1265–1287. doi: 10.5555/944919.944973
- 634 Doshi-Velez, F., & Kim, B. (2017). Towards a rigorous science of interpretable ma-
 635 chine learning. *arXiv preprint arXiv:1702.08608*. doi: 10.48550/arXiv.1702

636 .08608

- 637 Drucker, H. (1997). Improving regressors using boosting techniques. In *Icml*
638 (Vol. 97, pp. 107–115). doi: 10.5555/645526.657132
- 639 Dunkl, I., Lovenduski, N., Collalti, A., Arora, V. K., Ilyina, T., & Brovkin, V.
640 (2023). Gross primary productivity and the predictability of co₂: more uncer-
641 tainty in what we predict than how well we predict it. *Biogeosciences*, *20*(16),
642 3523–3538. doi: 10.5194/bg-20-3523-2023
- 643 Eyring, V., Bony, S., Meehl, G. A., Senior, C. A., Stevens, B., Stouffer, R. J., &
644 Taylor, K. E. (2016). Overview of the coupled model intercomparison project
645 phase 6 (cmip6) experimental design and organization. *Geoscientific Model*
646 *Development*, *9*(5), 1937–1958. doi: 10.5194/gmd-9-1937-2016
- 647 Fisher, R. A., & Koven, C. D. (2020). Perspectives on the future of land surface
648 models and the challenges of representing complex terrestrial systems. *Journal*
649 *of Advances in Modeling Earth Systems*, *12*(4), e2018MS001453. doi: 10.1029/
650 2018MS001453
- 651 Fisher, R. A., Koven, C. D., Anderegg, W. R., Christoffersen, B. O., Dietze, M. C.,
652 Farrior, C. E., ... others (2018). Vegetation demographics in earth system
653 models: A review of progress and priorities. *Global change biology*, *24*(1),
654 35–54. doi: 10.1111/gcb.13910
- 655 Friedlingstein, P., Meinshausen, M., Arora, V. K., Jones, C. D., Anav, A., Liddi-
656 coat, S. K., & Knutti, R. (2014). Uncertainties in cmip5 climate projections
657 due to carbon cycle feedbacks. *Journal of Climate*, *27*(2), 511–526. doi:
658 /10.1175/JCLI-D-12-00579.1
- 659 Gea-Izquierdo, G., Guibal, F., Joffre, R., Ourcival, J., Simioni, G., & Guiot, J.
660 (2015). Modelling the climatic drivers determining photosynthesis and carbon
661 allocation in evergreen mediterranean forests using multiproxy long time series.
662 *Biogeosciences*, *12*(12), 3695–3712. doi: 10.5194/bg-12-3695-2015
- 663 Goodfellow, I., Pouget-Abadie, J., Mirza, M., Xu, B., Warde-Farley, D., Ozair, S.,
664 ... Bengio, Y. (2020). Generative adversarial networks. *Communications of*
665 *the ACM*, *63*(11), 139–144. doi: 10.1145/3422622
- 666 Greenslade, M., Murphy, S., Treshansky, A., DeLuca, C., Guilyardi, E., & Denvil, S.
667 (2014). The earth system (es-doc) project. In *Egu general assembly conference*
668 *abstracts* (p. 12988).
- 669 Gültas, M., Düzgün, G., Herzog, S., Jäger, S. J., Meckbach, C., Wingender, E., &
670 Waack, S. (2014). Quantum coupled mutation finder: predicting function-
671 ally or structurally important sites in proteins using quantum jensen-shannon
672 divergence and cuda programming. *BMC bioinformatics*, *15*(1), 1–17. doi:
673 10.1186/1471-2105-15-96
- 674 Gutiérrez, J. M., Jones, R., Narisma, G., et al. (2021). Ipccl interactive at-
675 las. In *Climate change 2021: The physical science basis. contribution of*
676 *working group i to the sixth assessment report of the intergovernmental*
677 *panel on climate change*. Cambridge University Press Cambridge. doi:
678 10.1175/BAMS-D-20-0256.1
- 679 Guyon, I., & Elisseeff, A. (2003). An introduction to variable and feature selection.
680 *Journal of machine learning research*, *3*(Mar), 1157–1182. doi: 10.5555/944919
681 .944968
- 682 Guyon, I., Weston, J., Barnhill, S., & Vapnik, V. (2002). Gene selection for cancer
683 classification using support vector machines. *Machine learning*, *46*, 389–422.
684 doi: 10.1023/A:1012487302797
- 685 Hardouin, L., Delire, C., Decharme, B., Lawrence, D. M., Nabel, J. E., Brovkin, V.,
686 ... others (2022). Uncertainty in land carbon budget simulated by terrestrial
687 biosphere models: the role of atmospheric forcing. *Environmental Research*
688 *Letters*, *17*(9), 094033. doi: 10.1088/1748-9326/ac888d
- 689 Harper, A. B., Williams, K. E., McGuire, P. C., Duran Rojas, M. C., Hemming, D.,
690 Verhoef, A., ... others (2020). Improvement of modelling plant responses

- 691 to low soil moisture in Julesv4.9 and evaluation against flux tower mea-
692 surements. *Geoscientific Model Development Discussions*, 2020, 1–42. doi:
693 gmd-14-3269-2021
- 694 Huntingford, C., Jeffers, E. S., Bonsall, M. B., Christensen, H. M., Lees, T., & Yang,
695 H. (2019). Machine learning and artificial intelligence to aid climate change
696 research and preparedness. *Environmental Research Letters*, 14(12), 124007.
697 doi: 10.1088/1748-9326/ab4e55
- 698 Iturbide, M., Fernández, J., Gutiérrez, J. M., Pirani, A., Huard, D., Al Khourdajie,
699 A., ... others (2022). Implementation of fair principles in the ipcc: the wgi ar6
700 atlas repository. *Scientific data*, 9(1), 629. doi: 0.5281/zenodo.3691645
- 701 James, G., Witten, D., Hastie, T., Tibshirani, R., James, G., Witten, D., ... Tibshi-
702 rani, R. (2021). Linear regression. *An introduction to statistical learning: with*
703 *applications in R*, 59–128. doi: 10.1007/978-1-0716-1418-1_3
- 704 Jung, M., Koirala, S., Weber, U., Ichii, K., Gans, F., Camps-Valls, G., ... Reich-
705 stein, M. (2019). The fluxcom ensemble of global land-atmosphere energy
706 fluxes. *Scientific data*, 6(1), 1–14. doi: 10.1038/s41597-019-0076-8
- 707 Jung, M., Reichstein, M., Margolis, H. A., Cescatti, A., Richardson, A. D., Arain,
708 M. A., ... others (2011). Global patterns of land-atmosphere fluxes of carbon
709 dioxide, latent heat, and sensible heat derived from eddy covariance, satellite,
710 and meteorological observations. *Journal of Geophysical Research: Biogeo-*
711 *sciences*, 116(G3). doi: 10.1029/2010JG001566
- 712 Kanniah, K. D., Beringer, J., & Hutley, L. (2013). Exploring the link between
713 clouds, radiation, and canopy productivity of tropical savannas. *Agricultural*
714 *and Forest Meteorology*, 182, 304–313. doi: 10.1016/j.agrformet.2013.06.010
- 715 Kanniah, K. D., Beringer, J., & Hutley, L. B. (2011). Environmental controls
716 on the spatial variability of savanna productivity in the northern territory,
717 australia. *Agricultural and Forest Meteorology*, 151(11), 1429–1439. doi:
718 10.1016/j.agrformet.2011.06.009
- 719 Kelley, M., Schmidt, G. A., Nazarenko, L. S., Bauer, S. E., Ruedy, R., Russell,
720 G. L., ... others (2020). GISS-e2.1: Configurations and climatology. *Jour-*
721 *nal of Advances in Modeling Earth Systems*, 12(8), e2019MS002025. doi:
722 10.1029/2019MS002025
- 723 Kiang, N. (2012). *Description of the nasa giss vegetation dynamics model* (Tech.
724 Rep.). Tech. rep., NASA.
- 725 Kim, D., Lee, M.-I., Jeong, S.-J., Im, J., Cha, D. H., & Lee, S. (2018). Intercompar-
726 ison of terrestrial carbon fluxes and carbon use efficiency simulated by cmip5
727 earth system models. *Asia-Pacific Journal of Atmospheric Sciences*, 54(2),
728 145–163. doi: 10.1007/s13143-017-0066-8
- 729 Koch, A., Hubau, W., & Lewis, S. L. (2021). Earth system models are not cap-
730 turing present-day tropical forest carbon dynamics. *Earth’s Future*, 9(5),
731 e2020EF001874. doi: /10.1029/2020EF001874
- 732 Krinner, G., Viovy, N., de Noblet-Ducoudré, N., Ogée, J., Polcher, J., Friedlingstein,
733 P., ... Prentice, I. C. (2005). A dynamic global vegetation model for studies
734 of the coupled atmosphere-biosphere system. *Global Biogeochemical Cycles*,
735 19(1). doi: 10.1029/2003GB002199
- 736 Kumar, V., & Minz, S. (2014). Feature selection: a literature review. *SmartCR*,
737 4(3), 211–229. doi: 10.6029/smartcr.2014.03.007
- 738 LeCun, Y., Bengio, Y., & Hinton, G. (2015). Deep learning. *nature*, 521(7553), 436–
739 444. doi: doi.org/10.1038/nature14539
- 740 Levis, S. (2010). Modeling vegetation and land use in models of the earth system.
741 *Wiley Interdisciplinary Reviews: Climate Change*, 1(6), 840–856. doi: 10.1002/
742 wcc.83
- 743 Lin, J. (1991). Divergence measures based on the shannon entropy. *IEEE Transac-*
744 *tions on Information theory*, 37(1), 145–151. doi: 10.1109/18.61115
- 745 Mendes-Moreira, J., Soares, C., Jorge, A. M., & Sousa, J. F. D. (2012). Ensemble

- 746 approaches for regression: A survey. *Acm computing surveys (csur)*, 45(1), 1–
 747 40. doi: 10.1145/2379776.2379786
- 748 Molnar, C. (2020). *Interpretable machine learning*. Lulu. com.
- 749 Nishina, K., Ito, A., Falloon, P., Friend, A., Beerling, D., Ciais, P., . . . others
 750 (2015). Decomposing uncertainties in the future terrestrial carbon budget
 751 associated with emission scenarios, climate projections, and ecosystem simula-
 752 tions using the isi-mip results. *Earth System Dynamics*, 6(2), 435–445. doi:
 753 10.5194/esd-6-435-2015
- 754 Nzabarinda, V., Bao, A., Xu, W., Uwamahoro, S., Jiang, L., Duan, Y., . . . Long,
 755 G. (2021). Assessment and evaluation of the response of vegetation dyn-
 756 amics to climate variability in africa. *Sustainability*, 13(3), 1234. doi:
 757 10.3390/su13031234
- 758 on Climate Change, I. P. (2023). Global carbon and other biogeochemical cycles
 759 and feedbacks. In *Climate change 2021 – the physical science basis: Working*
 760 *group i contribution to the sixth assessment report of the intergovernmental*
 761 *panel on climate change* (p. 673–816). Cambridge University Press. doi:
 762 10.1017/9781009157896.007
- 763 O’Sullivan, M., Smith, W. K., Sitch, S., Friedlingstein, P., Arora, V. K., Haverd, V.,
 764 . . . others (2020). Climate-driven variability and trends in plant productivity
 765 over recent decades based on three global products. *Global Biogeochemical*
 766 *Cycles*, 34(12), e2020GB006613. doi: 10.1029/2020GB006613
- 767 Pedregosa, F., Varoquaux, G., Gramfort, A., Michel, V., Thirion, B., Grisel, O., . . .
 768 Duchesnay, E. (2011). Scikit-learn: Machine learning in Python. *Journal of*
 769 *Machine Learning Research*, 12, 2825–2830. doi: 10.5555/1953048.2078195
- 770 Quinlan, J. R. (1986). Induction of decision trees. *Machine learning*, 1, 81–106. doi:
 771 doi.org/10.1007/BF00116251
- 772 Reichler, T., & Kim, J. (2008). How well do coupled models simulate today’s cli-
 773 mate? *Bulletin of the American Meteorological Society*, 89(3), 303–312. doi:
 774 10.1175/BAMS-89-3-303
- 775 Righi, M., Andela, B., Eyring, V., Lauer, A., Predoi, V., Schlund, M., . . . others
 776 (2020). Earth system model evaluation tool (esmvaltool) v2. 0–technical
 777 overview. *Geoscientific Model Development*, 13(3), 1179–1199.
- 778 Santini, M., Collalti, A., & Valentini, R. (2014). Climate change impacts on vegeta-
 779 tion and water cycle in the euro-mediterranean region, studied by a likelihood
 780 approach. *Regional Environmental Change*, 14(4), 1405–1418.
- 781 Sarkar, D. P., Shankar, B. U., & Parida, B. R. (2022). Machine learning ap-
 782 proach to predict terrestrial gross primary productivity using topograph-
 783 ical and remote sensing data. *Ecological Informatics*, 70, 101697. doi:
 784 10.1016/j.ecoinf.2022.101697
- 785 Schapire, R. E. (2013). Explaining adaboost. *Empirical Inference: Festschrift in*
 786 *Honor of Vladimir N. Vapnik*, 37–52. doi: 10.1007/978-3-642-41136-6_5
- 787 Schimel, D. S., House, J. I., Hibbard, K. A., Bousquet, P., Ciais, P., Peylin, P., . . .
 788 others (2001). Recent patterns and mechanisms of carbon exchange by terres-
 789 trial ecosystems. *Nature*, 414(6860), 169–172. doi: 10.1038/35102500
- 790 Schlund, M., Eyring, V., Camps-Valls, G., Friedlingstein, P., Gentine, P., & Reich-
 791 stein, M. (2020). Constraining uncertainty in projected gross primary produc-
 792 tion with machine learning. *Journal of Geophysical Research: Biogeosciences*,
 793 125(11), e2019JG005619. doi: 10.1029/2019JG005619
- 794 Schwalm, C. R., Huntzinger, D. N., Michalak, A. M., Schaefer, K., Fisher, J. B.,
 795 Fang, Y., & Wei, Y. (2020). Modeling suggests fossil fuel emissions have
 796 been driving increased land carbon uptake since the turn of the 20th century.
 797 *Scientific Reports*, 10(1), 9059. doi: 10.1038/s41598-020-66103-9
- 798 Seddon, A. W., Macias-Fauria, M., Long, P. R., Benz, D., & Willis, K. J. (2016).
 799 Sensitivity of global terrestrial ecosystems to climate variability. *Nature*,
 800 531(7593), 229–232. doi: 10.1038/nature16986

- 801 S  ferian, R., Nabat, P., Michou, M., Saint-Martin, D., Voldoire, A., Colin, J., ...
802 others (2019). Evaluation of cnrm earth system model, cnrm-esm2-1: role of
803 earth system processes in present-day and future climate. *Journal of Advances*
804 *in Modeling Earth Systems*, 11(12), 4182–4227. doi: 10.1029/2019MS001791
- 805 Sellar, A. A., Jones, C. G., Mulcahy, J. P., Tang, Y., Yool, A., Wiltshire, A., ...
806 others (2019). Ukesm1: Description and evaluation of the uk earth system
807 model. *Journal of Advances in Modeling Earth Systems*, 11(12), 4513–4558.
808 doi: 10.1029/2019MS001739
- 809 Smola, A. J., & Sch  lkopf, B. (2004). A tutorial on support vector regression. *Statist-*
810 *ics and computing*, 14, 199–222. doi: 10.1023/B:STCO.0000035301.49549.88
- 811 Spafford, L., & MacDougall, A. H. (2021). Validation of terrestrial biogeochemistry
812 in cmip6 earth system models: a review. *Geoscientific Model Development*,
813 14(9), 5863–5889. doi: gmd-14-5863-2021
- 814 Sun, Y., Frankenberg, C., Wood, J. D., Schimel, D., Jung, M., Guanter, L., ...
815 others (2017). Oco-2 advances photosynthesis observation from space via
816 solar-induced chlorophyll fluorescence. *Science*, 358(6360), eaam5747. doi:
817 10.1126/science.aam57
- 818 Swart, N. C., Cole, J. N., Kharin, V. V., Lazare, M., Scinocca, J. F., Gillett,
819 N. P., ... others (2019). The canadian earth system model version 5
820 (canesm5. 0.3). *Geoscientific Model Development*, 12(11), 4823–4873. doi:
821 10.5194/gmd-12-4823-2019
- 822 Varghese, R., & Behera, M. (2019). Annual and seasonal variations in gross primary
823 productivity across the agro-climatic regions in india. *Environmental monitor-*
824 *ing and assessment*, 191(10), 631. doi: 10.1007/s10661-019-7796-2
- 825 Verma, A., Chandel, V., & Ghosh, S. (2022). Climate drivers of the variations
826 of vegetation productivity in india. *Environmental Research Letters*, 17(8),
827 084023. doi: 10.1088/1748-9326/ac7c7f
- 828 Versegny, D. (2012). Class—the canadian land surface scheme (version 3.6). *Environ-*
829 *ment Canada Science and Technology Branch Tech. Rep*, 176.
- 830 Wu, D., Zhao, X., Zhao, W., Tang, B., & Xu, W. (2014). Response of vegetation to
831 temperature, precipitation and solar radiation time-scales: A case study over
832 mainland australia. In *2014 ieee geoscience and remote sensing symposium*
833 (pp. 855–858). doi: 10.1109/IGARSS.2014.6946559
- 834 Wu, Z., Ahlstr  m, A., Smith, B., Ard  , J., Eklundh, L., Fensholt, R., & Lehsten, V.
835 (2017). Climate data induced uncertainty in model-based estimations of ter-
836 restrial primary productivity. *Environmental Research Letters*, 12(6), 064013.
837 doi: 10.1088/1748-9326/aa6fd8
- 838 Yang, L., & Shami, A. (2020). On hyperparameter optimization of machine learn-
839 ing algorithms: Theory and practice. *Neurocomputing*, 415, 295–316. doi: /10
840 .1016/j.neucom.2020.07.061
- 841 Yao, Y., Wang, X., Li, Y., Wang, T., Shen, M., Du, M., ... others (2018). Spa-
842 tiotemporal pattern of gross primary productivity and its covariation with
843 climate in china over the last thirty years. *Global Change Biology*, 24(1),
844 184–196.
- 845 Yu, T., Zhang, Q., & Sun, R. (2021). Comparison of machine learning methods to
846 up-scale gross primary production. *Remote Sensing*, 13(13), 2448. doi: 10
847 .3390/rs13132448
- 848 Zampieri, M., Grizzetti, B., Toreti, A., De Palma, P., & Collalti, A. (2021). Rise and
849 fall of vegetation annual primary production resilience to climate variability
850 projected by a large ensemble of earth system models’ simulations. *Environ-*
851 *mental Research Letters*, 16(10), 105001. doi: 10.1088/1748-9326/ac2407
- 852 Zarakas, C. M., Swann, A. L., Lagu  , M. M., Armour, K. C., & Randerson, J. T.
853 (2020). Plant physiology increases the magnitude and spread of the transient
854 climate response to co2 in cmip6 earth system models. *Journal of Climate*,
855 33(19), 8561–8578. doi: 10.1175/JCLI-D-20-0078.1

- 856 Zhang, F., Lu, X., Huang, Q., & Jiang, F. (2022). Impact of different era reanaly-
857 sis data on gpp simulation. *Ecological Informatics*, 68, 101520. doi: 10.1016/
858 j.ecoinf.2021.101520
- 859 Zhang, Y., Joiner, J., Alemohammad, S. H., Zhou, S., & Gentine, P. (2018).
860 A global spatially contiguous solar-induced fluorescence (csif) dataset us-
861 ing neural networks. *Biogeosciences*, 15(19), 5779–5800. doi: 10.5194/
862 bg-15-5779-2018
- 863 Zhang, Z., Xin, Q., & Li, W. (2021). Machine learning-based modeling of vegetation
864 leaf area index and gross primary productivity across north america and com-
865 parison with a process-based model. *Journal of Advances in Modeling Earth*
866 *Systems*, 13(10), e2021MS002802. doi: 10.1029/2021MS002802